Novel Force Estimation Method for Magnetic Lead Screw-Based RotLin Actuator

Lang Bu, *Member, IEEE*, and Yasutaka Fujimoto, *Senior Member, IEEE*

***Abstract*—This article proposes a method to precisely estimate the load force of magnetic lead screw (MLS)-based series elastic actuators (SEAs) in real time. The elastic transmissions of MLS-based SEAs generally comprise permanent magnets (PMs). Owing to the magnetic pole distortion and the characteristic nonlinear force of PMs, conventional force estimation methods are less accurate for MLS-based actuators than for SEAs with mechanical springs. In the proposed method, to precisely estimate force of MLSs, the nonlinear force characteristic of an MLS is modeled with a sinusoidal force model, and the magnetic force hysteresis phenomenon is predicted based on Bouc–Wen-type hysteresis equations. Moreover, a method called the relative displacement normalization method is proposed to detect the magnetic pole distortion and to compensate for the related force estimation error. In addition, the proposed method is applied to a rotary-linear (RotLin) actuator, which is a novel MLS-based linear SEA. The force estimation accuracy is experimentally evaluated by comparison with existing methods. The results demonstrate that the root-mean-square error of the proposed method is less than that of the existing polynomial model by up to 81.2%. Finally, a force controller and a static force control system is designed with the proposed model to prove its feasibility.**

***Index Terms*—Force estimation, magnetic lead screw (MLS), nonlinear distortion, rotary-linear (RotLin) actuator, series elastic actuator (SEA).**

I. Introduction

SERIES elastic actuators (SEAs) have been widely applied in human–robot interaction owing to its inherent compliance and force sensibility [1], [2]. However, the mechanical springs and transmissions in linear SEAs cause problems such as backlash, friction, and nonbackdrivability. Magnetic lead screws (MLSs) have recently drawn much attention because of their ability to convert small torques into large forces without direct contact between the rotor and translator. The structure of an ideal MLS is shown in Fig. 1. Compared with mechanical SEAs, it has the advantages of low friction, inherent backdrivability, inherent overload protection, no backlash, and low maintenance. Moreover, compared with conventional permanent magnet (PM) actuators, it has a higher force density. Additionally, as a radial-gap actuator, it does not require gap control, which is necessary in axial gap actuators (e.g., the spiral motor proposed in [3] and [4]). Previous studies have focused on improving the thrust force, constructing an ideal helix magnetic field, simplifying the manufacture, or reducing the cost of MLSs. However, the real-time force estimation of MLSs has rarely been considered.

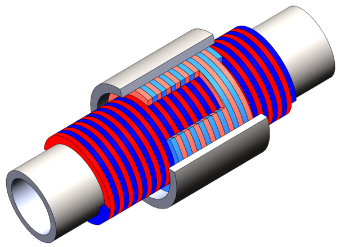

Fig. 1. Section view of an ideal MLS.

Novel MLSs and actuators have been designed for different applications in recent years. A high-temperature superconductor electromagnetic screw (HTS-EMS) [5] and a Halbach magnetized magnetic screw [6] were designed for an artificial heart. Furthermore, a 500 kN MLS was designed for wave energy conversion, and a 17 kN demonstrator was built for verification [7]. To reduce cost, a moving-magnet-type interior permanent MLS (MM-IPMLS) was proposed [8] with a screw made of a soft magnetic material that is easy to extend and discrete arc-shaped PMs that are easy to manufacture. Moreover, a magnetically geared lead screw with no magnets on the translator was proposed [9] to reduce cost in a long-stroke application. Additionally, a new MLS structure [10] that can well approximate helical magnetic poles with discrete PMs was proposed. A compact direct-drive linear actuator integrating a rotary machine and a magnetic screw was also designed [11], where the magnetic circuits were decoupled. In addition, some studies have focused on the theoretical analysis of MLSs. Wang et al. [12] proposed a unified framework to predict the thrust force of tubular linear actuators based on field solutions. Analytical and numerical analyses were performed to predict the performance of MLSs [13]. The effects of pole count and stack length on the gear ratio and force characteristics were studied [14]. In terms of optimization of the system cost and weight of the linear actuator, the superiority

Manuscript received 24 February 2022; revised 6 June 2022; accepted 18 July 2022. Date of publication 29 July 2022; date of current version 21 November 2022. This work was supported in part by Grant-in-Aid for Scientific Research (KAKENHI) under Grant 21H01306. Paper 2022-IDC-0212.R1, presented at the 2020 IEEE Energy Conversion Congress and Exposition (ECCE), Portland, MI, USA, Oct. 11–15, and approved for publication in the IEEE TRANSACTIONS ON INDUSTRY APPLICATIONS by the Industrial Drives Committee of the IEEE Industry Applications Society. *(Corresponding author: Lang Bu.)*

Lang Bu is with the Department of Electrical and Computer Engineering, Yokohama National University, Yokohama 240-8501, Japan (e-mail: langbu_92@hotmail.com).

Yasutaka Fujimoto is with the Department of Electrical and Computer Engineering, Yokohama National University, Yokohama 240-8501, Japan (e-mail: fujimoto@ynu.ac.jp).

Color versions of one or more figures in this article are available at https://doi.org/10.1109/TIA.2022.3194867.

Digital Object Identifier 10.1109/TIA.2022.3194867

of a trans-rotary magnetic gear (TROMAG) integrated rotary machine over a conventional direct-drive linear PM machine in high-force low-speed reciprocating motion applications was proven [15].

Although the force characteristics of MLSs have been widely analyzed, estimating the force in real time remains challenging. A previously proposed disturbance observer (DOB) [16], [17] provides the possibility of estimating the force from the rotor-side disturbance; however, the needs of the rotor-side friction model and the low-pass filter decrease the accuracy and slow down the speed of the observation. In addition, the widely used finite-element analysis (FEA) method (e.g., in [5]–[15]) is unsuitable for real-time force estimation. The previously reported force analysis [12], [13] provides a way to predict the thrust force of ideal MLSs, but it is difficult to use for real-time force estimation because of the massive calculation and the lack of consideration of field distortion. Although a real-time force estimation method was proposed and evaluated using MM-IPMLS [8], this method requires a premeasured force curve and polynomial approximation to determine parameters, which weakens its practicability. Moreover, the method neglects the distortion of magnetxsxtsic poles.

The real-time force estimation is essential in force control, where SEAs show their superiority: the force of a conventional SEA can be easily estimated from the deformation of the mechanical spring. However, for MLS-based actuators, the conventional force estimation method is inaccurate owing to the characteristic nonlinear force and magnetic pole distortion of PMs. The present article, as an extension research of [1], proposes a novel real-time force estimation method, and evaluated the method with the designed MLS-based rotary-linear (RotLin) actuator and control system. The proposed method is distinct from existing methods in the following aspects.

1) A sinusoidal force model with easily determined parameters is introduced to estimate the nonlinear magnetic force of MLSs.
2) Bouc–Wen-type equations are used to predict the magnetic force hysteresis phenomenon of MLSs.
3) A method to detect the magnetic field distortion of MLSs and an estimation error compensation method based on relative displacement normalization (RDN) are proposed.

It is worth mentioning that although the original purpose of the proposed method is to enhance the force estimation accuracy of the RotLin actuator, the method is applicable to other MLS-based actuators. In particular, it can significantly improve the force estimation accuracy of MLSs with distinct magnetic-field distortion. It provides an alternative way to improve the force characteristics of MLSs, in addition to increasing the number of discrete PM blocks, as reported previously [18], which makes manufacturing difficult.

The rest of this article is organized as follows. Section II introduces the structure, modeling, and force analysis of the RotLin actuator. Section III discusses the components of the proposed force estimation method in detail. Section IV presents the experimental results. Section V discusses the universality of the method. Finally, Section VI concludes this article.

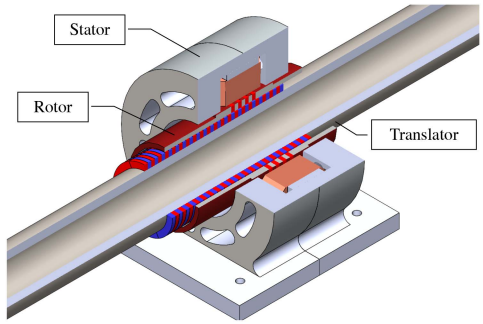

Fig. 2. Section view of the RotLin actuator.

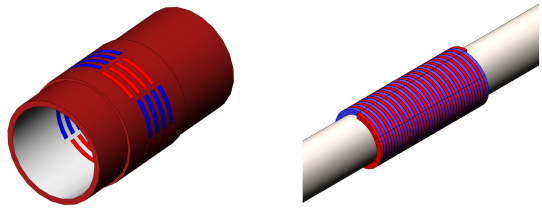

Fig. 3. MLS of the RotLin actuator. (a) Rotor and (b) translator.

II. MLS-Based Direct-Drive RotLin Actuator

In contrast to other MLS-based actuators that connect a motor with MLS in series, the RotLin actuator is a compact direct-drive linear actuator that combines the stator of a PM brushless dc motor (BLDCM) with an MLS in the radial direction. The structure, principle, modeling, and force characteristics of the RotLin actuator are discussed in this section.

A. Structure of the RotLin Actuator

As shown in Fig. 2, the RotLin actuator consists of three main parts: the stator, rotor, and translator. The stator with 12 slots adopting concentrating winded coils has a structure similar to the stator of a BLDCM. The PMs on the rotor and the translator are helical and radially magnetized. The rotor frame shown in Fig. 3(a) is made of Bakelite. This nonferromagnetic material ensures that the rotor is lightweight and compact while freeing the actuator from the cogging torque between the rotor frame and the translator. The PMs embedded in the rotor have four poles in the axial direction and eight poles in the tangential direction. The surface PMs on the translator are composed of discrete helical PMs with a 60° arc, as shown in Fig. 3(b).

The previously built prototype of the RotLin actuator in [19] is shown in Fig. 4. The mover, which is a combination of the rotor and stator connected by ball bearings, is supported by linear guides. The translator is fixed to a base plate with shaft holders. The mover and rotor are equipped with a linear encoder and rotary encoder, respectively. A force sensor is installed at the load side for evaluation. The measured dimensional parameters of the RotLin prototype are presented in Fig. 5 and Table I.

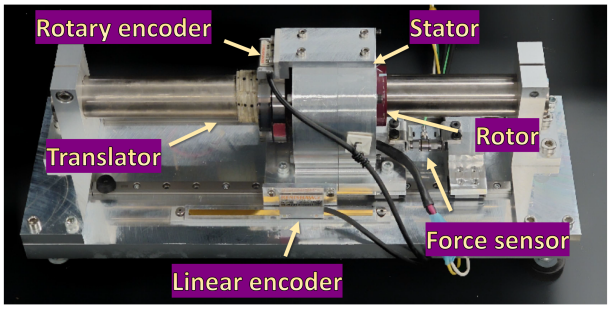

Fig. 4. Prototype of RotLin actuator.

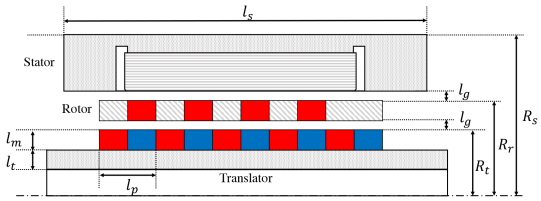

Fig. 5. Dimensional parameters of the RotLin actuator.

TABLE I
DIMENSIONAL PARAMETERS OF THE ROTLIN ACTUATOR

Description	Symbol	Value
Outer radius of the stator [mm]	R_s	47.25
Outer radius of the rotor [mm]	R_r	26.25
Outer radius of the translator [mm]	R_t	17.45
Radial length of the PMs [mm]	l_m	2.5
Radial length of the translator [mm]	l_t	7.5
Radial length of the air gaps [mm]	l_g	0.8
Radial length of the stator [mm]	l_s	65
Pitch length [mm]	l_p	5.1429
Axial pole number of the rotor	p_a	4
Tangential pole number of the rotor	p_t	8

B. SEA Model of the RotLin Actuator

An MLS-based actuator is essentially an atypical SEA in which the mechanical elastic transmissions are replaced by a magnetic spring. In applications involving low thrust force, the magnetic spring force was approximately linearized as follows:

$$F_s = K_s x_d \tag{1}$$

where K_s is the spring constant of the linearized force model. x_d is the relative displacement between the rotor and the translator and was expressed as follows:

$$x_d = h\theta - x \tag{2}$$

where x and θ represent the mover displacement and rotor angle, respectively. h is the transfer ratio from rotary to linear motion and was expressed as follows:

$$h = l_p/2\pi. \tag{3}$$

Taking J as the inertia of the rotor and M as the mass of the mover, the kinematic equations were derived as follows:

$$J\ddot{\theta} = T - T_s \tag{4}$$

$$M\ddot{x} = F_s - F_l \tag{5}$$

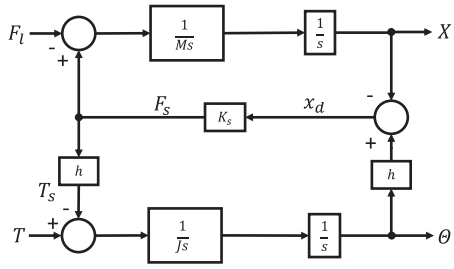

Fig. 6. Conventional SEA model of the RotLin actuator.

where T and T_s represent the electromagnetic torque and feedback spring torque on the rotor, respectively. F_l represents the load force. According to energy conservation, the relationship between the spring force and spring torque was derived as follows:

$$T_s = hF_s. \tag{6}$$

The conventional SEA model of the RotLin actuator was built [20] based on (1)–(6), as shown in Fig. 6.

C. Magnetic Force Analysis

To predict the force performance of MLSs, an analytical and numerical method was adopted previously [12], [13]. It was concluded that for an ideal MLS with infinite-permeability back irons and an axially symmetric and periodic field distribution, the axial force acting on one pole of the rotor magnets is as follows:

$$F = 4\pi J_c \sum_{n=1,2,\ldots} K_n \sin\left(m_n x_p\right) \tag{7}$$

where x_p represents the axial displacement between the poles on the rotor and the translator. J_c is the equivalent current density of the rotor magnets, which was obtained from follows:

$$J_c = \frac{B_{rem}}{\mu_r \mu_0} \tag{8}$$

where B_{rem} is the remanence of the PMs and μ_r and μ_0 are the relative recoil permeability of the magnets and permeability of the space, respectively. K_n and m_n are constant parameters related to the nth component of the flux density. Details of the calculation are provided in the original paper.

For the RotLin actuator with p_a axial poles on the rotor, when the pole distortion is neglected, the pole displacement x_p is equal to x_d, and the thrust force of the RotLin actuator was derived as follows:

$$F = 4\pi p_a J_c \sum_{n=1,2,\ldots} K_n \sin\left(m_n x_d\right). \tag{9}$$

The analytical thrust force of the RotLin actuator with respect to the relative displacement is shown in Fig. 7 in comparison with the linearized model based on (1) and the measurement result from the force sensor.

The results demonstrate that the estimation error of the linear model starts to become significant when the force is greater than 100 N, indicating that the widely used linear model of SEAs is applicable to MLSs only under low force. The analytical

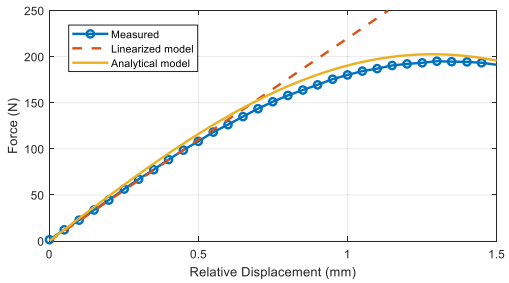

Fig. 7. Measured, linearized, and analytical thrust force of the RotLin actuator.

model can better predict the thrust force over the entire range. However, a gap still exists between the analytical and measured values. This could be a result of the effect of saturation, which is neglected in the model, as reported by Wang et al. [13].

III. Proposed Real-Time Force Estimation Method

This section introduces the proposed real-time force estimation method for an MLS-based actuator. The three components of this method, namely, the sinusoidal force model, hysteresis model, and error compensation method based on RDN, are discussed in detail. In addition, a load force observer (LFOB) is designed for experimental evaluation.

A. Sinusoidal Force Model

The analytical model expressed by (9) is a summation equation with n components, and the calculation of K_n is massive. However, the components with $n > 1$ are very small; for example, for the RotLin actuator, the ratio between K_2 and K_1 is 1.58%, and the ratio between K_3 and K_1 is 0.08%. Considering that the components with $n > 1$ are neglected, (9) was simplified as follows:

$$F_s = 4\pi p_a J_c K_1 \sin\left(m_1 x_d\right). \tag{10}$$

In (10), the product of the coefficients before the sine function and m_1 are constants, which implies that the magnetic force related to the relative displacement is almost sinusoidal. Therefore, a sinusoidal force model was assumed as follows:

$$F_s = a \sin\left(b x_d\right) \tag{11}$$

where a and b are constant parameters need to be determined. Taking F_{stall} as the stall force of MLS, the corresponding relative displacement is one quarter of the pitch length, that is

$$F_{stall} = a \sin\left(b l_p/4\right) \tag{12}$$

$$b l_p/4 = \pi/2. \tag{13}$$

Solution of (12) and (13) yields $a = F_{stall}$ and $b = 2\pi/l_p$, and the sinusoidal model expressed by h follows:

$$F_s = F_{stall} \sin\left(x_d/h\right). \tag{14}$$

In this sinusoidal model, h is a dimensional parameter that can be easily determined. The only parameter that needs to be identified is the stall force, which can be determined from an overload test.

B. Hysteresis Model Based on Bouc–Wen-Type Equations

Magnetic hysteresis occurs when the pole distance between the rotor and translator of an MLS varies. Consequently, the force of MLSs is not only related to the relative displacement at any moment, but also to that in the past. Therefore, a static model cannot precisely describe the force characteristics of MLSs. Previously [21], a Bouc–Wen-type hysteresis model was applied to model the torsion-torque hysteresis of elastic-joint robots. Although the principles of magnetic force hysteresis and mechanical torsion-torque hysteresis are different, their performances are similar. Therefore, it is possible to model the magnetic hysteresis of the MLS-based RotLin actuator with modified Bouc–Wen-type equations.

The torsion-torque hysteresis based on the Bouc–Wen-type hysteresis model of the ith joint follows:

$$\tau_i\left(\Delta_i\right) = \sum_i k_{i,j}\left(w_i \Delta_i^j + \left(1 - w_i\right) x_i^j\right) \tag{15}$$

where k_j, with $j = \{1, 3\}$, represents the linear and cubic stiffness coefficients; $w_i \in [0, 1]$ is the weighting factor between the purely elastic $(w_i = 1)$ and purely plastic $(w_i = 0)$ hysteresis behaviors; and Δ_i represents the joint torsion of the ith joint. x_i is an internal state that captures the hysteresis behavior follows:

$$\dot{x}_i = \phi_i \dot{\Delta}_i - \psi_i |\dot{\Delta}_i| \left|x_i\right|^{\eta_i - 1} x_i - \xi_i \dot{\Delta}_i \left|x_i\right|^{\eta_i} \tag{16}$$

where ϕ_i, $\psi_i > 0$, $\eta_i \geq 0$, and $\xi \geq 1$ are parameters that adjust the shape of the hysteresis curve. Details are discussed elsewhere [22].

Equation (15) was modified to estimate hysteresis forces of MLS-based actuators. For an actuator with one MLS, the summation in (15) is not needed. Moreover, Δ_i^j, representing the torsion of the ith joint, was replaced with relative displacement of an MLS: x_d. The product of $k_{i,j}$ and Δ_i^j, which represents the linear torsion-torque of one joint, was replaced with magnetic spring force of an MLS, expressed with the proposed sinusoidal force model: $F_{stall} \sin(x_d/h)$. From these modification, the hysteresis model for MLS-based actuators was developed as follows:

$$F_s(x_d) = F_{stall}[w \sin\left(x_d/h\right) + (1 - w) \sin\left(x_s/h\right)] \tag{17}$$

where x_s is an internal state similar to (16) as follows:

$$\dot{x}_s = \phi \dot{x}_d - \psi |\dot{x}_d| \left|x_s\right|^{\eta - 1} x_s - \xi_s \dot{x}_d \left|x_s\right|^{\eta}. \tag{18}$$

F_{stall} and h control the scale of hysteresis loop in the vertical and horizontal directions, respectively. The modeled hysteresis loops related to parameters w, F_{stall} and h are shown in Fig. 8(a)–(c), respectively.

The identification results of the hysteresis model of the RotLin actuator are shown in Fig. 9. The overall hysteresis loop is shown in Fig. 9(a). The gray arrow lines in sequence of AB, BC and CD indicate the directions of force variation. The details around the zero point are shown in Fig. 9(b), where an overlapping part exists between Curves A–B and C–D in the region indicated with a blue arrow. The identified parameters are shown in Table II.

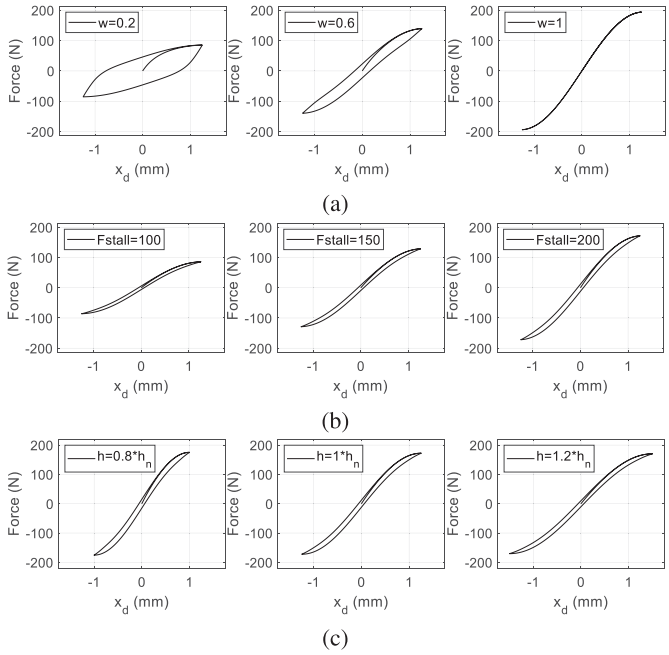

Fig. 8. Modeled hysteresis loops related to (a) w, (b) F_{stall}, and (c) x_d.

TABLE II
PARAMETERS RELATED TO THE EVALUATION EXPERIMENT

Description	Symbol	Value
Nominal torque constant	K_{tn}	0.0387 N·m/A
Nominal mass of the mover	M_n	2.55 kg
Nominal inertia of the rotor	J_n	7.68×10^{-5} kg·m^2
Cutoff frequency of DOB	g_D	1000 rd/s
Cutoff frequency of LFOB	g_L	200 rd/s
Cutoff frequency of speed calculator	g_v	1000 rd/s
Spring constant of linear model	K_s	220×10^3 N/m
Position controller	K_p	100
Speed controller	K_v	0.5
Nominal transfer ratio	h_n	8.19×10^{-4} m/rad
Stall force	F_{stall}	192 N
Weight factor of hysteresis model	w	0.96
Stiff coefficient of load	K_e	2250 N/m
Damping coefficient of load	D_e	0.1 N·s/m
Internal state parameters of the hysteresis model	ϕ	1
	ψ	3000
	ξ	1000
	η	1
Parameters of the modified Coulomb friction model	γ_1	0.8
	γ_2	200
	γ_3	0.05

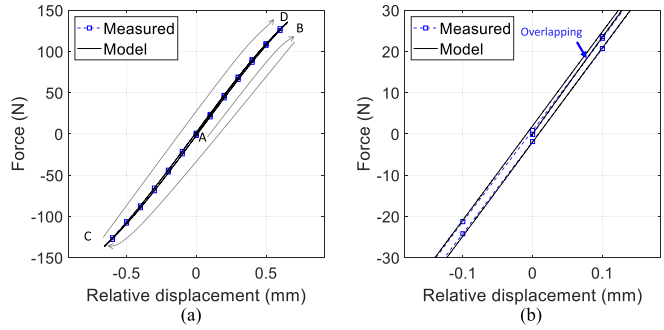

Fig. 9. Proposed hysteresis model. (a) Overall hysteresis loop and (b) details around zero point.

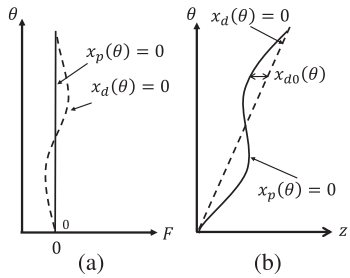

Fig. 10. Diagram of $x_d = 0$ and $x_p =$ of an MLS with discrete PMs in (a) θ-F coordinate and (b) θ-z coordinate.

C. Magnetic Pole Distortion Detection and RDN Method

According to the analysis in (7), the thrust force of an MLS is related to the pole distance. For an ideal MLS with helix poles, the pole distance is equal to the relative displacement, that is, $x_p = x_d$. However, to simplify the manufacturing process, most MLS designs adopt discrete PMs. The discrete poles and the deviation of the polarization of the PM blocks lead to magnetic pole distortion. Consequently, $x_p \neq x_d$, resulting in a force estimation error. If x_d is normalized to x_p, the estimation errors related to magnetic pole distortion can be compensated. Assuming a variable $x_{d0}(\theta)$, the following equation can be formulated:

$$x_{d0}(\theta) = x_d(\theta) - x_p(\theta) \tag{19}$$

The normalized relative displacement x_{dn} satisfies the following relationship:

$$x_{dn}(\theta) = x_d(\theta) - x_{d0}(\theta). \tag{20}$$

To identify the $x_{d0}(\theta)$, the concept of zero-force line was introduced. From (7), when $x_p = 0$, force of an MLS equals zero. Therefore, the zero-force line, representing by $x_p = 0$, shows the position where force between shaft and rotor in the z direction equals zero. $x_p = 0$ is a straight line in the θ-F coordinate, as shown in Fig. 10(a). Differently, x_d is related to the structure of an MLS, and $x_d = 0$ is a straight line in θ-z coordinate, as shown in Fig. 10(b). The lines represented by $x_d = 0$ and $x_p = 0$ are consistent only when the MLS is ideal, as shown in Fig. 11, where the pole distortions of discrete PMs are illustrated through the varying shades of color. By detecting the difference between $x_d = 0$ and $x_p = 0$ in z direction, $x_{d0}(\theta)$ can be identified.

To identify x_{d0}, a simple identification experiment that does not require a force sensor is designed. First, the actuator is controlled to move forward and backward at the same constant speed, and the relative displacements are recorded as $x_{df}(\theta)$ and $x_{db}(\theta)$, respectively. To simplify the equations, a linearized model is used to describe the small spring force, and the dynamic equations of the mover using normalized relative displacements

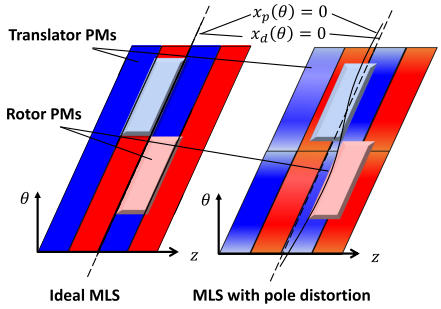

Fig. 11. Diagram of ideal and distorted zero-force lines.

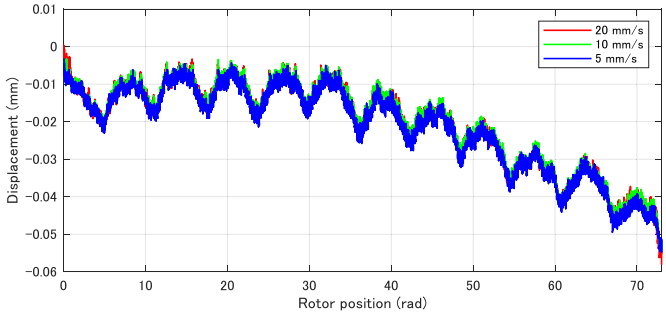

Fig. 12. Identification of x_{d0} identified under different speeds of 5 (blue), 10 (green), and 20 mm/s (red).

were as follows:

$$K_s(x_{df}(\theta) - x_{d0}(\theta)) - F_{ff} = 0 \tag{21}$$

$$K_s(x_{db}(\theta) - x_{d0}(\theta)) - F_{fb} = 0 \tag{22}$$

where F_{ff} and F_{fb} are the frictions during the forward and backward movements, respectively. As the speeds in the two directions have the same constant value, the friction values are related as follows:

$$F_{ff} = -F_{fb}. \tag{23}$$

With (21)–(23), the variable to normalize the relative displacement was determined

$$x_{d0}(\theta) = \frac{x_{df}(\theta) + x_{db}(\theta)}{2}. \tag{24}$$

The identification experiment of x_{d0} was conducted under different speeds of 20, 10, and 5 mm/s, and the results are shown in Fig. 12. The results show that the identified x_{d0} values under different speeds are almost identical, proving that the zero-force line related to the rotor position is independent of speed. In addition, the identified x_{d0} reflects the characteristics of pole distortion. For instance, the periodic pattern of x_{d0} with a periodicity equal to the rotor rotation turns is related to the magnetic pole distortion on the rotor, whereas the overall variation of x_{d0} is related to the magnetic pole distortion on the translator. This experiment can detect pole distortion due to imperfectly polarized PMs, manufacturing errors, and/or nonstandard MLS structure design.

By replacing x_d in the sinusoidal hysteresis model expressed by (17) and (18) with x_{dn} expressed by (20), the proposed force model was derived as

$$F_s(x_d) = F_{stall}[w \sin(x_{dn}/h) + (1-w)\sin(x_s/h)] \tag{25}$$

where x_s is an internal state following

$$\dot{x}_s = \phi \dot{x}_{dn} - \psi |\dot{x}_{dn}| \, |x_s|^{\eta-1} x_s - \xi_s \dot{x}_{dn} \, |x_s|^{\eta}. \tag{26}$$

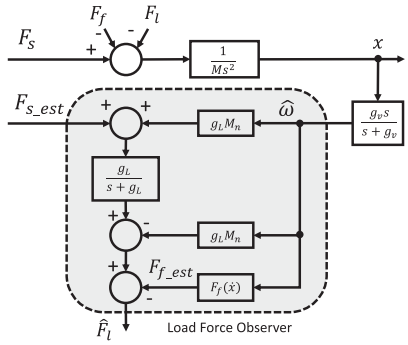

Fig. 13. LFOB with the modified Coulomb friction model.

D. Design of Load Force Observer

The direct measurement of the spring force associated with an MLS is difficult, owing to no contact between the mover and stator. Therefore, the comparison of the estimated spring force and the measurement is difficult. To evaluate the accuracy of the proposed method, an LFOB with a structure similar to a DOB, proposed by Ohnishi et al. [23] was designed (see Fig. 13). The primary difference between the designed LFOB and a conventional LFOB is the methods applied for obtaining the spring force and friction. The designed LFOB estimated the spring force through proposed method. The load force was estimated by subtracting the friction from the observed load-side disturbance as follows:

$$\hat{F}_l = (F_{s\_est} + g_L M_n \hat{\omega}) \frac{g_L}{g_L + s} - g_L M_n \hat{\omega} - F_{f\_est} \tag{27}$$

where $\hat{\omega}$ is the estimated speed of mover expressed as follows:

$$\hat{\omega} = \frac{g_v s}{g_v + s} x \tag{28}$$

g_L and g_v are the cutoff frequency of the low-pass filter of the LFOB and speed calculator, respectively. M_n is the nominal mass of the mover, and F_{s_est} is the spring force estimated from the proposed force model. F_{f_est} is the mover-side friction estimated from the modified Coulomb friction model

$$F_f(\dot{x}) = \gamma_1 \tanh(\gamma_2 \dot{x}) + \gamma_3 \operatorname{sign}(\dot{x}) \tag{29}$$

where γ_1 and γ_3 represent viscous friction and Coulomb friction, respectively. γ_2 is a coefficient that adjusts the pre-slide performance of the friction model when the speed is near zero.

IV. Experimental Evaluation

The proposed force estimation method was experimentally evaluated. The experiment platform was built based on an inverter unit MWINV-5R022 and a control board PE-F28335 A, procured from Myway Plus corporation. The control board

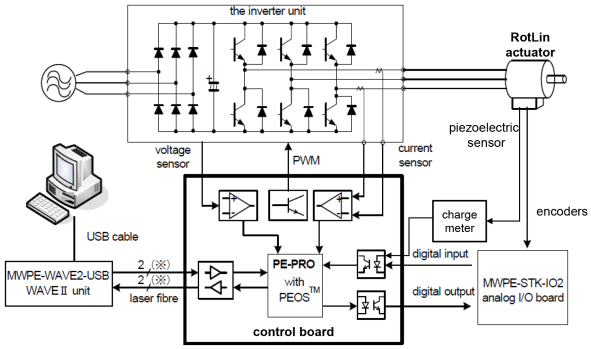

Fig. 14. Experiment setup configuration diagram.

equips a microcontroller TMS320F28335PGFA with a clock frequency of 150 MHz. The carrier frequency of the control signal was set to 10 000 Hz. The control system was programmed with the software Code Composer Studio ver.5.0 software, in C codes. The PE-View 9 Software was used for processes such as compiling, downloading execution/stopping. Rotary encoders T2011-10 A and linear encoders RGH24X30D00 A from Renishaw corporation are used for angle and displacement measurement, respectively. Piezoelectric sensor and charge amplifier type 5015, used for load force measurement, were from Kistler corporation. Fig. 14 shows the experimental setup.

The parameters related to the control system and the models are listed in Table II. In our previous research, a rotor position control based proportional controllers and DOB was included [1]. The rotor position system was applied for the experimental evaluation. The experiments were divided into static and dynamic evaluations. In the static evaluation, the sinusoidal and hysteresis models were evaluated. In the dynamic evaluation, the proposed force estimation method was evaluated and compared with existing methods. Finally, a force controller was designed and combined with the position control system.

A. *Static Evaluation of Sinusoidal and Hysteresis Model*

The static evaluation results of the proposed sinusoidal force model expressed by (14) are shown in Fig. 15. The results show that the sinusoidal model is consistent with the measured force and the maximum error is approximately 2 N.

To evaluate the accuracy and robustness of the hysteresis model against the variation of the magnetic field and force, experiments were conducted in different positions under different force scales (see Figs. 16–18). In addition, errors of estimation with and without hysteresis model are compared. The results show that even in situations different from the identification experiment, the model can still estimate the force hysteresis and improve the accuracy of force estimation.

B. *Dynamic Evaluation of the Proposed Method*

The proposed force estimation method was experimentally evaluated in the dynamic states. In the experiments, plastic foam based elastic loads were applied, where the mover interacts

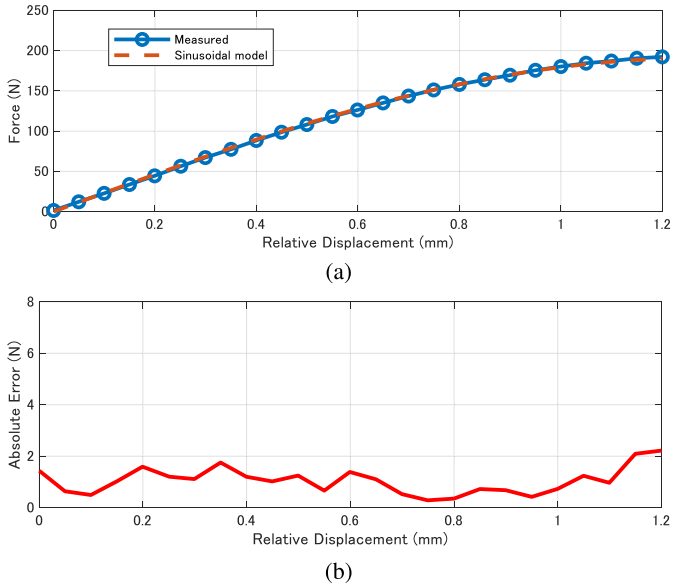

Fig. 15. Static evaluation of the sinusoidal model. (a) Estimated and measured thrust forces and (b) absolute estimation error.

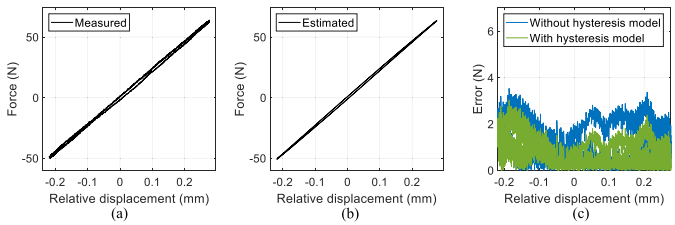

Fig. 16. Position 1—maximum force at 75 N (approximate). (a) Measured, (b) estimated, and (c) error.

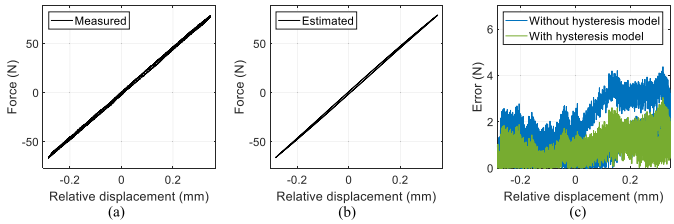

Fig. 17. Position 2—maximum force at 75 N (approximate). (a) Measured, (b) estimated, and (c) error.

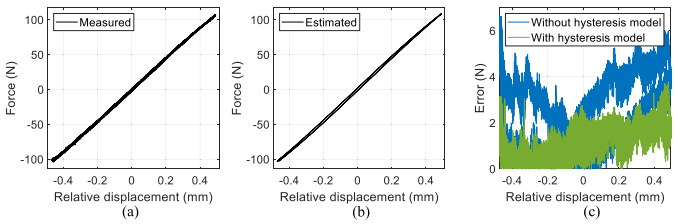

Fig. 18. Position 2—maximum force at 165 N (approximate). (a) Measured, (b) estimated, and (c) error.

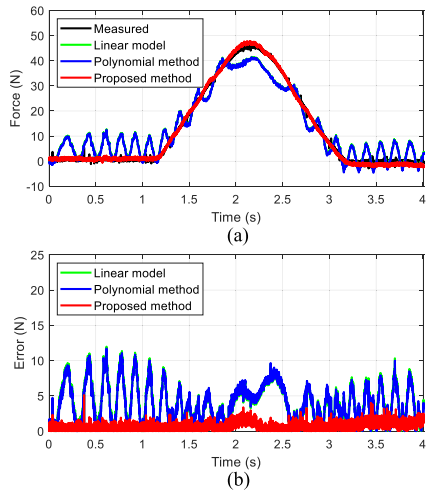

Fig. 19. Experiment 1. (a) Estimation results. (b) Absolute errors.

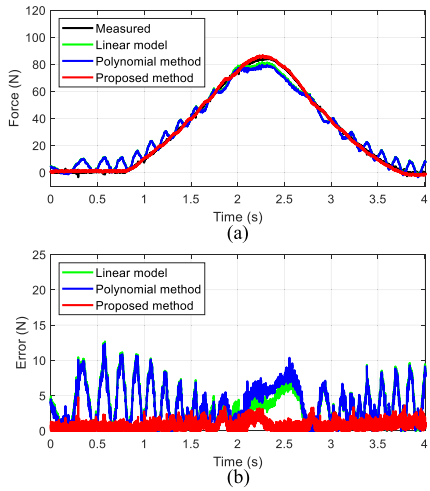

Fig. 20. Experiment 2. (a) Estimation results. (b) Absolute errors.

TABLE III
RMSEs [N] (RATE RATIO) OF DIFFERENT METHODS

Experiment	Polynomial	Linear	Proposed
1	4.68 N (100%)	4.77 N (101.9%)	0.88 N (18.8%)
2	4.65 N (100%)	4.48 N (96.4%)	0.99 N (21.3%)
3	4.14 N (100%)	7.23 N (174.5%)	1.62 N (39.1%)

with the load along a sinusoidal movement. The results were compared with two existing force estimation methods: a conventional linear model and a polynomial model. Figs. 19–21 show the three experiments conducted under maximum load forces at approximately 45, 85, and 165 N, respectively, Furthermore, the estimation results and absolute errors of the three methods were compared. The root-mean-square errors (rmses) of the three methods in the three experiments are listed in Table III.

The results show that the accuracy of linear model and polynomial model are almost identical when the load force is less than 100 N. The polynomial method shows superiority over the linear model under a load force greater than 100 N. However, both methods suffer from errors with a periodic pattern. This pattern associated with pole distortions of PMs is consistent with the pattern of zero-force line detection results shown in Fig. 12. The proposed method shows the best accuracy thanks to the hysteresis model and the RDN method.

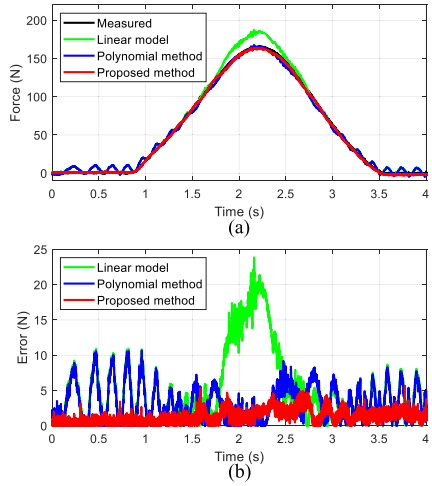

Fig. 21. Experiment 3. (a) Estimation results. (b) Absolute errors.

C. Force Control System Design and Evaluation

To verify the feasibility of the proposed model in force control and its generality in terms of combining with conventional systems, a static force controller and a force control system were designed and evaluated experimentally. In the static state, the load side forces follows:

$$F_{\text{stall}} \sin\left[\left(h\theta - x - x_{d0}\right)/h\right] - F_l - F_f = 0. \tag{30}$$

From (30), a force controller for generating rotor position reference from load force reference is designed as

$$\theta_{ref} = \sin^{-1} \frac{F_l^{ref} + F_{f\_est}}{F_{\text{stall}}} + \frac{1}{h}\left(x + x_{d0}\right) \tag{31}$$

where x_{d0} and F_{f_est} are determined from the proposed zero-force line identification method and the modified friction model, respectively. A force control system combining the force controller and a conventional position control with proportional controllers and DOB is designed, as shown in Fig. 22.

To derive the transfer function of the designed system, the nonlinear force model was linearized. Around an arbitrary point, $x_d = x_d^*$ and $F_s = F_s^*$, the coefficient K_l^* of a linearized force model was derived from (14) as follows:

$$K_l^* = \frac{F_s - F_s^*}{x_d - x_d^*} = \frac{F_{stall}}{h}\cos(x_d^*/h). \tag{32}$$

The Laplace transform of (32) yields

$$F_s(s) = K_l^* x_d(s). \tag{33}$$

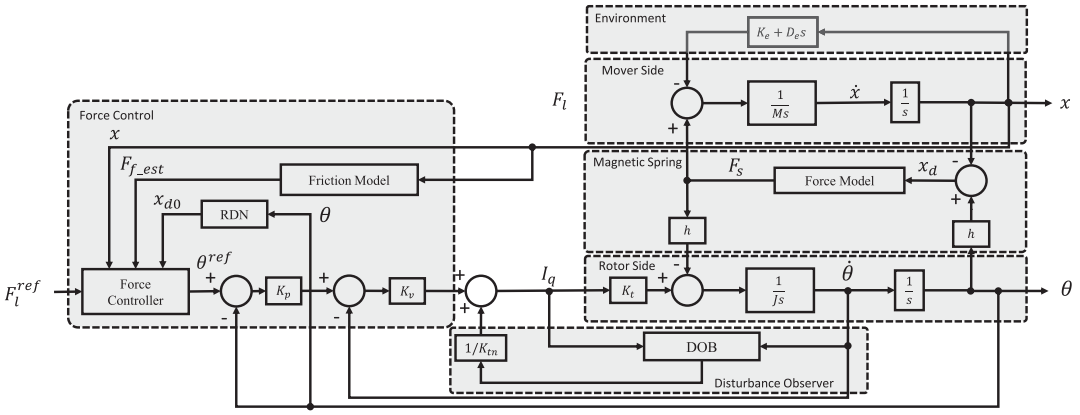

Fig. 22. Control block of the designed force control system.

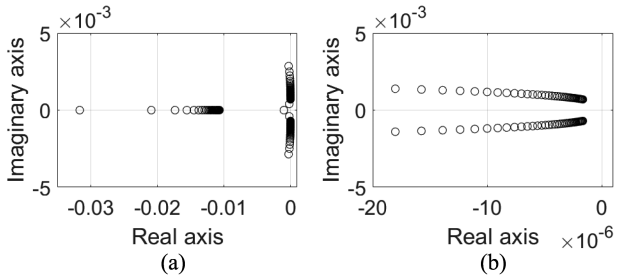

Fig. 23. Locus of poles along variation of K_e, from 0 to 5000 kN/m. (a) Overall and (b) details around zero point.

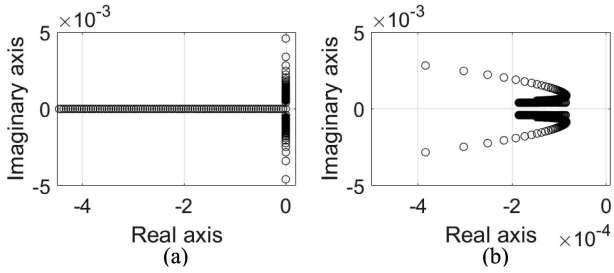

Fig. 24. Locus of poles along variation of K_l^*, from 0 to 10 000 kN/m. (a) Overall and (b) details around zero point.

Considering environment impedance as $K_e + D_e s$, the load force is obtained as follows:

$$F_l = (K_e + D_e s)x \tag{34}$$

where K_e and D_e represent the stiffness and damping coefficients of the environment, respectively; the transfer function from the force reference to the load force is derived as follows:

$$\frac{F_l(s)}{F_l^{ref}(s)} = \frac{Num(s)}{Den(s)} \tag{35}$$

The numerator Num and denominator Den are provided in the appendix. The stability of the designed system was verified using Routh–Hurwitz criterion. By taking nominal values of the system into (35), the components in the first column of Routh–Hurwitz criterion table, as functions of variables K_l^* and K_e, were derived. The results demonstrate that with any positive value of K_e and K_l^*, the Routh–Hurwitz criterion is satisfied. The locus of poles along the variation of K_e, and K_l^* are shown in Figs. 23 and 24, respectively, indicating all the poles have negative real parts.

The results of the force control evaluation experiments are shown in Fig. 25. The load was a soft object composed of plastic foam, and the reference forces were set to 50 and 100 N in Fig. 25(a) and (b), respectively. The corresponding absolute errors are shown in Fig. 25(c) and (d), respectively. The results demonstrate that the system was stable and error was small, indicating the feasibility of the proposed force control system.

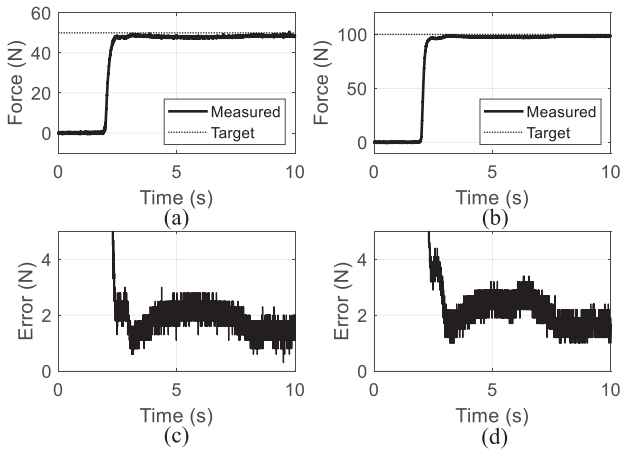

Fig. 25. Experimental results of force control: (a) 50 N force control, (b) 100 N force control, (c) error of 50 N force control, and (d) error of 100 N force control.

V. Discussion

Although the proposed force estimation method was designed for the RotLin actuator, it is a universal method for MLS-based linear actuators. The model includes a sinusoidal model, a hysteresis model, and RDN to overcome three common problems in the force estimation of MLSs: the inherent nonlinear force characteristic, magnetic hysteresis, and magnetic pole distortion. The three components of the force model do not necessarily work together, which means that each model can also work with or be

replaced by other models. For instance, the polynomial model proposed in [8] can be improved by adopting RDN. Alternatively, for actuators in which magnetic hysteresis is insignificant, it is acceptable to remove the hysteresis model to simplify the system. Moreover, because the proposed RDN method does not include any specific magnetic field model, it is a universal method that is applicable to MLSs with different designs. This shows the ability of the proposed method to improve the force estimation accuracy of MLSs, especially for those with relatively large PM blocks and nonideal helical distributed poles.

VI. Conclusion

In this article, a novel method for estimating the thrust force of MLSs was proposed. Each component of the method was introduced in detail: the static force model based on the sinusoidal model to estimate the static nonlinear force of an MLS; a hysteresis model based on Bouc–Wen-type hysteresis equations to predict the magnetic force hysteresis; and a compensation method based RDN to compensate for the estimation error owing to the pole distortion of PMs. An LFOB was designed for evaluation experiments. Moreover, a static force controller was designed and combined with a conventional position control system.

The accuracy of the proposed static sinusoidal model and hysteresis model was evaluated with static experiments. The dynamic experiments demonstrate that the proposed method reduces the rmse of force estimation by up to 81.2%, in comparison with the existing polynomial model. Static force control experiments verified the feasibility and generality of combining with existing control system.

This article focused on the improvement of the force estimation accuracy of MLSs and MLS-based actuators through a preliminary control system design. We expect to extend this research in the future, toward system improvement, the analysis of robustness, and disturbances response. In addition, the proposed method is expected to be applied to MLS-based actuators other than the RotLin actuator.

Appendix

$$\begin{aligned} Num = {} & g_D g_v K_e K_p K_t K_v + (D_e g_D g_v K_p K_t K_v \\ & + g_D K_e K_p K_t K_v + g_v K_e K_p K_t K_v)s \\ & + (D_e g_D K_p K_t K_v + D_e g_v K_p K_t K_v \\ & + K_e K_p K_t K_v)s^2 + (D_e K_p K_t K_v)s^3 \end{aligned} \tag{36}$$

$$\begin{aligned} Den = {} & g_D g_v K_e K_p K_t K_v + (g_v h^2 K_e K_l^* + g_D g_v K_e K_t K_v \\ & + g_D g_v K_l^* K_t K_v + D_e g_D g_v K_p K_t K_v + g_D K_e K_p K_t K_v \\ & + g_v K_e K_p K_t K_v)s + (g_D g_v J K_e + D_e g_v h^2 K_l^* \\ & + g_D g_v J K_l^* + h^2 K_e K_l^* + D_e g_D g_v K_t K_v + g_v K_e K_t K_v \\ & + g_v K_l^* K_t K_v + D_e g_D K_p K_t K_v + D_e g_v K_p K_t K_v \\ & + K_e K_p K_t K_v + g_D g_v K_p K_t K_v M)s^2 + (D_e g_D g_v J \\ & + g_D J K_e + g_v J K_e + D_e h^2 K_l^* + g_D J K_l^* + g_v J K_l^* \\ & + D_e g_v K_t K_v + D_e K_p K_t K_v + g_v h^2 K_l^* M \\ & + g_D g_v K_t K_v M + g_D K_p K_t K_v M + g_v K_p K_t K_v M)s^3 \\ & + (D_e g_D J + D_e g_v J + J K_e + J K_l^* + g_D g_v J M \\ & + h^2 K_l^* M + g_v K_t K_v M + K_p K_t K_v M)s^4 + (D_e J \\ & + g_D J M + g_v J M)s^5 + J M s^6. \end{aligned} \tag{37}$$

References

[1] L. Bu and Y. Fujimoto, "A robust position control system based on load force observer for rotlin machine," in *Proc. IEEE Energy Convers. Congr. Expo.*, 2020, pp. 1134–1139.

[2] A. Calanca, R. Muradore, and P. Fiorini, "A review of algorithms for compliant control of stiff and fixed-compliance robots," *IEEE/ASME Trans. Mechatronics*, vol. 21, no. 2, pp. 613–624, Apr. 2016.

[3] Y. Fujimoto, T. Kominami, and H. Hamada, "Development and analysis of a high thrust force direct-drive linear actuator," *IEEE Trans. Ind. Electron.*, vol. 56, no. 5, pp. 1383–1392, May 2009.

[4] A. Z. Shukor and Y. Fujimoto, "Direct-drive position control of a spiral motor as a monoarticular actuator," *IEEE Trans. Ind. Electron.*, vol. 61, no. 2, pp. 1063–1071, Feb. 2014.

[5] Z. Ling, W. Zhao, J. Ji, J. Zhu, and J. Mao, "Design and analysis of a new HTS electromagnetic screw," *IEEE Trans. Magn.*, vol. 53, no. 11, pp. 1–4, Nov. 2017.

[6] J. Ji, Z. Ling, J. Wang, W. Zhao, G. Liu, and T. Zeng, "Design and analysis of a halbach magnetized magnetic screw for artificial heart," *IEEE Trans. Magn.*, vol. 51, no. 11, pp. 1–4, Nov. 2015.

[7] R. K. Holm, N. I. Berg, M. Walkusch, P. O. Rasmussen, and R. H. Hansen, "Design of a magnetic lead screw for wave energy conversion," *IEEE Trans. Ind. Appl.*, vol. 49, no. 6, pp. 2699–2708, Nov./Dec. 2013.

[8] A. Heya, Y. Nakata, M. Sakai, H. Ishiguro, and K. Hirata, "Force estimation method for a magnetic lead-screw-driven linear actuator," *IEEE Trans. Magn.*, vol. 54, no. 11, pp. 1–5, Nov. 2018.

[9] M. B. Kouhshahi, J. Z. Bird, J. D. Kadel, and W. B. Williams, "Designing and experimentally testing a magnetically geared lead screw," *IEEE Trans. Ind. Appl.*, vol. 54, no. 6, pp. 5736–5747, Nov./Dec. 2018.

[10] Z. Ling, W. Zhao, J. Ji, and G. Liu, "Design of a new magnetic screw with discretized PMs," *IEEE Trans. Appl. Supercond.*, vol. 26, no. 4, pp. 1–5, Jun. 2016.

[11] Z. Ling, W. Zhao, P. O. Rasmussen, J. Ji, Y. Jiang, and Z. Liu, "Design and manufacture of a linear actuator based on magnetic screw transmission," *IEEE Trans. Ind. Electron.*, vol. 68, no. 2, pp. 1095–1107, Feb. 2021.

[12] J. Wang, G. Jewell, and D. Howe, "A general framework for the analysis and design of tubular linear permanent magnet machines," *IEEE Trans. Magn.*, vol. 35, no. 3, pp. 1986–2000, May 1999.

[13] J. Wang, K. Atallah, and W. Wang, "Analysis of a magnetic screw for high force density linear electromagnetic actuators," *IEEE Trans. Magn.*, vol. 47, no. 10, pp. 4477–4480, Oct. 2011.

[14] S. Pakdelian, N. W. Frank, and H. A. Toliyat, "Principles of the trans-rotary magnetic gear," *IEEE Trans. Magn.*, vol. 49, no. 2, pp. 883–889, Feb. 2013.

[15] S. Pakdelian, Y. B. Deshpande, and H. A. Toliyat, "Design of an electric machine integrated with trans-rotary magnetic gear," *IEEE Trans. Energy Convers.*, vol. 30, no. 3, pp. 1180–1191, Sep. 2015.

[16] A. Kato and K. Ohnishi, "Robust force sensorless control in motion control system," in *Proc. IEEE 9th Int. Workshop Adv. Motion Control*, 2006, pp. 165–170.

[17] Y. Ohba, S. Katsura, and K. Ohishi, "Sensor-less force control for machine tool using reaction torque observer," in *Proc. IEEE Int. Conf. Ind. Technol.*, 2006, pp. 860–865.

[18] Z. Ling, J. Ji, J. Wang, and W. Zhao, "Design optimization and test of a radially magnetized magnetic screw with discretized PMs," *IEEE Trans. Ind. Electron.*, vol. 65, no. 9, pp. 7536–7547, Sep. 2018.

[19] C. S. Cyusa and Y. Fujimoto, "Enactment-based direct-drive test of a novel radial-gap helical rotlin machine," *IEEE Trans. Ind. Appl.*, vol. 54, no. 2, pp. 1273–1282, Mar./Apr. 2018.

[20] L. Bu and Y. Fujimoto, "Sensor-less back-driving control of direct-drivable rotlin linear series elastic actuator," in *Proc. 47th Annu. Conf. IEEE Ind. Electron. Soc.*, 2021, pp. 1–5.

[21] M. Ruderman and M. Iwasaki, "Sensorless torsion control of elastic-joint robots with hysteresis and friction," *IEEE Trans. Ind. Electron.*, vol. 63, no. 3, pp. 1889–1899, Mar. 2016.

[22] F. Ma, H. Zhang, A. Bockstedte, G. C. Foliente, and P. Paevere, "Parameter analysis of the differential model of hysteresis," *J. Appl. Mech.*, vol. 71, no. 3, pp. 342–349, 2004.
[23] K. Ohishi, "Torque-speed regulation of DC motor based on load torque estimation," in *Proc. IEEJ Int. Power Electron. Conf.*, 1983, vol. 2, pp. 1209–1216.

Lang Bu (Member, IEEE) was born in Heilongjiang, China. He received the B.E. degree in electrical engineering and automation, and the M.E. degree in physical electronics from Southwest Jiaotong University, Sichuan, China, in 2014 and 2018, respectively. He is currently working toward the Ph.D. degree in electrical and computer engineering with Yokohama National University, Yokohama, Japan.

His present work focuses on development of a novel 2-degree-of-freedom actuator for robotic exoskeleton with high force density and force sensibility. His research interests include motion control, robotics, and electrical machine design.

Yasutaka Fujimoto (Senior Member, IEEE) was born in Kanagawa, Japan. He received the B.E., M.E., and Ph.D. degrees in electrical and computer engineering from Yokohama National University, Yokohama, Japan, in 1993, 1995, and 1998, respectively.

In 1998, he was with the Department of Electrical Engineering, Keio University, Yokohama, Japan. Since 1999, he has been with the Department of Electrical and Computer Engineering, Yokohama National University, where he is currently a Professor. His research interests include actuators, robotics, manufacturing automation, and motion control.

Dr. Fujimoto is a member of Robotics Society of Japan. He was the recipient of IEEE/ASME TRANSACTION ON MECHATRONICS Best Paper Award in 2020. He is an Associate Editor for IEEE TRANSACTIONS ON INDUSTRIAL ELECTRONICS and a Vice Chief for IEEJ Journal of Industry Applications. (Based on document published on 23 October 2020).